Feasibility Study of Dose Reduction in Digital Breast Tomosynthesis Using Non-Local Denoising Algorithms

Marcelo A. C. Vieira*[a], Helder C. R. de Oliveira[a], Polyana F. Nunes[a], Lucas R. Borges[a], Predrag R. Bakic[b], Bruno Barufaldi[a,b], Raymond J. Acciavatti[b], Andrew D. A. Maidment[b]

[a] Department of Electrical Engineering, University of São Paulo, São Carlos, SP, Brazil
[b] Department of Radiology, University of Pennsylvania, Philadelphia, PA, USA

ABSTRACT

The main purpose of this work is to study the ability of denoising algorithms to reduce the radiation dose in Digital Breast Tomosynthesis (DBT) examinations. Clinical use of DBT is normally performed in "combo-mode", in which, in addition to DBT projections, a 2D mammogram is taken with the standard radiation dose. As a result, patients have been exposed to radiation doses higher than used in digital mammography. Thus, efforts to reduce the radiation dose in DBT examinations are of great interest. However, a decrease in dose leads to an increased quantum noise level, and related decrease in image quality. This work is aimed at addressing this problem by the use of denoising techniques, which could allow for dose reduction while keeping the image quality acceptable. We have studied two "state of the art" denoising techniques for filtering the quantum noise due to the reduced dose in DBT projections: Non-local Means (NLM) and Block-matching 3D (BM3D). We acquired DBT projections at different dose levels of an anthropomorphic physical breast phantom with inserted simulated microcalcifications. Then, we found the optimal filtering parameters where the denoising algorithms are capable of recovering the quality from the DBT images acquired with the standard radiation dose. Results using objective image quality assessment metrics showed that BM3D algorithm achieved better noise adjustment (mean difference in peak signal to noise ratio < 0.1dB) and less blurring (mean difference in image sharpness ~ 6%) than the NLM for the projections acquired with lower radiation doses.

Keywords: Digital breast tomosynthesis, dose reduction, image denoising, non-local means, block-matching 3D.

1. INTRODUCTION

Digital Breast Tomosynthesis (DBT) is a novel x-ray medical imaging modality in which a limited number of low dose projections from a narrow angular range are acquired as the x-ray tube moves over an arc.[1] A 3D volume is reconstructed from these projections and tomographic sections of the breast are generated. The advantage over 2D digital mammography is that tomosynthesis reduces the tissue superposition, which could impair the visibility of lesions.[2] In 2011, the Food and Drug Administration (FDA) allowed the clinical use of DBT in the United States in "combo-mode", in which, in addition to the projections, a 2D mammography was taken with the standard radiation dose.[3] As a result, patients have been exposed to radiation doses higher than used in digital mammography. Efforts to reduce the radiation dose in DBT examinations are of great interest because of the patient's risk of radiation-induced cancer.[4,5] However, a decrease in the dose leads to an increased quantum noise level in the image, which potentially affects diagnostic performance.[6,7]

This work is aimed at assessing the feasibility of the use of denoising techniques, which could allow for dose reduction while keeping the image quality acceptable. We investigated two "state of the art" denoising techniques: Non-Local Means (NLM)[8] and Block Matching 3D (BM3D)[9], which have been applied to a set of DBT projections acquired at different radiation dose levels, lower than the regular dose used in clinical examinations. Selected quantitative measures of image quality were used to estimate the percentage of dose reduction that, in combination with denoising techniques, would produce images of comparable quality as those acquired with the full radiation dose.

*mvieira@sc.usp.br; phone +55-16-3373-9353; fax +55-16-3373-9372; www.sel.eesc.usp.br

Medical Imaging 2015: Physics of Medical Imaging, edited by Christoph Hoeschen, Despina Kontos,
Proc. of SPIE Vol. 9412, 94122C · © 2015 SPIE · CCC code: 1605-7422/15/$18 · doi: 10.1117/12.2082398

2. METHODOLOGY

2.1 Non-local means

Buades *et al*. first presented the Non-Local Means (NLM) algorithm in 2005.[8] Unlike conventional denoising techniques, the NLM does not take into account only the local characteristics of the image when calculating the estimated denoised value of a pixel; it also considers the self-similarities that can be found in natural images. To do so, the algorithm gives different weights to identified similar patches and calculates the estimated value of the noiseless pixels by averaging these patches.

Let $v = \{v(i) |\ i \in I\}$ be the noisy image. The estimated noiseless image, $\hat{v}$ is calculated by:[8]

$$\hat{v} = \sum\nolimits_{j \in I} [w(i,j)v(j)] \tag{1}$$

where $\{w(i,j)\}_j$ are the weights for each patch, satisfying the following conditions: $0 \le w(i,j) \le 1$ and $\sum_j w(i,j) = 1$.

The weights are calculated considering the distance between each chosen patch $v(N_j)$ and the patch being processed $v(N_i)$, using the following equation:[8]

$$w(i,j) = \frac{1}{Z(i)}\, e^{\frac{-\,\|v(N_i) - v\,(N_j)\|_{2,a}^{2}}{h^2}} \tag{2}$$

where h is a parameter used to control the amount of noise to be removed by the filter and $Z(i)$ is a function used for normalization, given by:[8]

$$Z(i) = \sum_j e^{\frac{-\,\|v(N_i) - v\,(N_j)\|_{2,a}^{2}}{h^2}} \tag{3}$$

2.2 Block-matching 3D

The Block-Matching 3D (BM3D) algorithm was originally proposed by Dabov *et al.* in 2007.[9] This algorithm works in two basic steps. In the first step, it creates a preliminary estimate of a noiseless image using a wavelet-based denoising algorithm, which works grouping similar patches into a 3D stack. A square window of size n is selected from the image and inside this area a patch (P) with size $k^{hard}\ x\ k^{hard}$ is used as reference. Every other patch (Q) taken from this area is compared with the reference (P) using the Euclidian distance between them, as shown in Equation (4):[9]

$$d(P,Q) = \frac{\|\gamma'(P) - \gamma'(Q)\|_2^2}{(k^{\mathrm{hard}})^2} \tag{4}$$

where γ' is the operator of hard-thresholding in wavelet domain. The threshold value normally is chosen based on the standard deviation of the noise (σ).

Whether the distance $d(P,Q)$ is less than a selected threshold (τ^{hard}), the patch (Q) is considered as part of that stack $\mathcal{P}(P)$. Therefore, $\mathcal{P}(P)$ can be described as:[9]

$$\mathcal{P}(\mathrm{P}) = \{\mathrm{Q}: \mathrm{d}(\mathrm{P},\mathrm{Q}) \le \tau^{\mathrm{hard}}\} \tag{5}$$

In the second step, after creating the 3D groups, the wavelet transform is applied again to each patch, creating a sparse representation of the stack. After that, a hard-thresholding is applied along the third dimension of the stack. Finally, the wavelet inverse transform is performed and the result is processed to avoid problems with borders and artifacts. The pre-estimate of the noiseless image, $u^{basic}(x)$, can then be calculated by the following expression:[9]

$$u^{basic}(x) = \frac{\sum_{P} w_P^{hard} \sum_{Q \in P(P)} \chi_Q(x) u_{Q,P}^{hard}(x)}{\sum_{P} w_P^{hard} \sum_{Q \in P(P)} \chi_Q(x)} \tag{6}$$

where $\mathrm{w_P^{hard}}$ controls what is the priority given to homogeneous patches, $\mathrm{u_{Q,P}^{hard}}$ is the estimated pixel x, which belongs to the patch Q and was obtained by the collaborative filtering of the reference patch P, and $\chi_\mathrm{Q}(\mathrm{x})$ is a binary function where if $\mathrm{x} \in \mathrm{Q}$, then $\chi_\mathrm{Q}(\mathrm{x}) = 1$, else $\chi_\mathrm{Q}(\mathrm{x}) = 0$.

The second step is the collaborative Wiener filtering. This step uses the same method for matching patches into 3D blocks that were used in the first step. The pre-estimate image, $\mathrm{u^{basic}(x)}$, is used as a reference to the Wiener filtering in order to generate the final estimate of the denoised image.

2.3 Image acquisition

In order to evaluate the denoising methodology, a set of DBT projections was acquired using an anthropomorphic physical breast phantom,[10] prototyped by CIRS, Inc. (Reston, VA) with a license from the University of Pennsylvania (Penn). The breast phantom consists of six slabs, each containing simulated anatomical structures manufactured using tissue mimicking materials, based upon a realization of the breast software phantom developed at Penn.[11] The phantom simulates a 450 ml breast, compressed to 5 cm, with 17% volumetric breast density (excluding the skin). In addition to the normal breast anatomy, for the purpose of this work, simulated microcalcifications were included in the phantom. The cluster was simulated using Calcium Oxalate (99%, Alfa Aesar, Ward Hill, MA). Individual pieces of Calcium Oxalate of different sizes (ranging from 106μm to 2000μm) were sieved and placed on a piece of single-sided Scotch tape, to mimic a cluster. The tape with simulated cluster was positioned between slabs of the physical phantom before imaging. Figure 1(a) shows a photograph of all slabs of the anthropomorphic breast phantom used in this study. One of the simulated microcalcifications clusters can be seen in Figure 1(b), which is an enlarged photograph of the rightmost slab at Figure 1(a).

(a) (b)

Figure 1 – Anthropomorphic physical breast phantom used for acquiring DBT images to evaluate the denoising algorithms.

A set of phantom images was acquired using a clinical DBT machine (Selenia Dimensions, Hologic, Bedford, MA). First, we acquired a set of 15 DBT projections using the Automatic Exposure Control mode (AEC) of the clinical machine. This acquisition provides us all the optimized parameters automatically set for this phantom. Then, we switch to Manual mode and acquired five sets (with 15 projections each) using the same parameters provided by the AEC mode. This was done to guarantee that all set of images were acquired using the same exposition parameters. This set was called "100% dose", as it represents the images acquired using the standard radiation dose provided by the equipment. Then, we altered the "*current x time*" parameter (*mAs*) in order to obtain set of images in different doses, holding all the other parameters provided for the AEC mode. Using this approach, we acquired DBT projections at 4 different doses: 100%, 85%, 70% and 50% of the regular dose, changing only the mAs between the expositions. For each case, we acquired a group of 5 DBT images, in order to get different noise realizations for each one of the radiation doses. At the end, we generated a database with 300 images: 15 projections at each acquisition × 4 different doses × 5 acquisitions at each dose.

Moreover, we acquired 10 additional projections sets of the physical phantom using the same parameters as for the 100% dose group. These images were averaged to obtain a good approximation of a noiseless image. This image was used as a *ground-truth* for all the image quality measurements conducted in this study. These sets were acquired separately from the initial 5 sets at 100% dose to avoid quality assessment bias.

Tomographic slices were generated from all synthetic projections using a commercial DBT reconstruction software[12] (Briona™ 3D, Real-Time Tomography, LLC, Villanova, PA). This software uses a filtered back projection algorithm to generate reconstructed slices on planes parallel to the breast support at various depths of the breast volume. For this study, we generated slices 1.0 mm thick on a slice spacing of 1.0 mm.

Figure 2 shows an example of the DBT images acquired with the anthropomorphic breast phantom: shown on the left is an example of the central projection (acquisition angle = 0°) and on the right an example of a reconstructed slice. The black arrows indicate the location of one simulated microcalcification cluster.

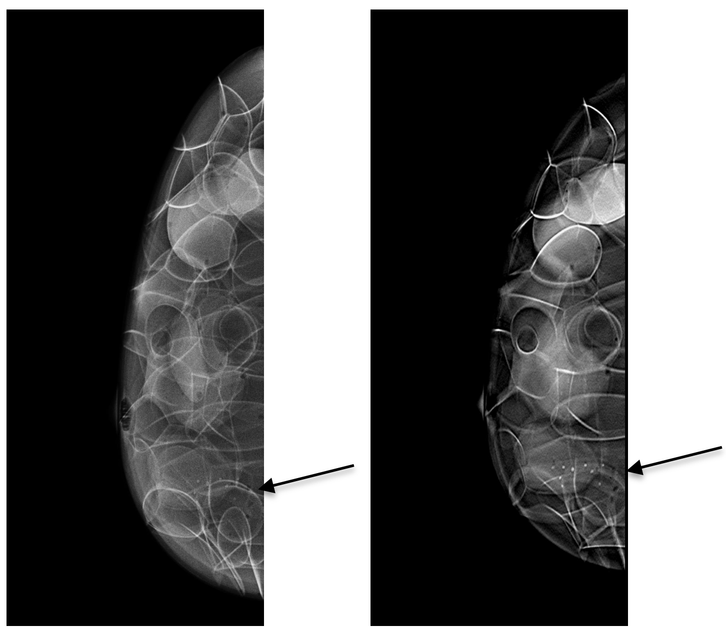

Figure 2 – Examples of DBT images acquired with the anthropomorphic physical breast phantom: a) central projection; b) reconstructed slice. The black arrows indicate the location of one simulated microcalcification cluster.

2.4 Image Quality Descriptors

We considered some objective image quality metrics to evaluate image quality before and after denoising and also to adjust filter parameters. Objective measurements were performed by the calculation of the following image quality metrics: peak of signal-to-noise ratio (PSNR),[13] mean structural similarity index (MSSIM)[14] and sharpness.[15]

The PSNR represents the ratio between the maximum possible power of a signal and the power of the corrupting noise that affects the fidelity of its representation. Typically, the PSNR value is given in decibels (dB) and a higher PSNR would normally indicate denoising of higher quality.[13] The MSSIM index includes human visual perception in the measurement by extracting information about the luminance, contrast and structure of an image. It was designed to improve traditional signal-fidelity measures. Structural similarity index (SSIM) is calculated on various windows, which should be displaced pixel-by-pixel in the image. In practice, the mean value of the SSIM indexes (MSSIM) of all windows is used to evaluate the overall image quality. The resultant MSSIM index is a value between -1 and 1, where a value of 1 can be reached only in the case of two identical images.[14] Both PSNR and MSSIM are full reference image quality assessment metrics, i.e., a reference image (ground-truth) is necessary to calculate those parameters, as they compare two signals by providing a quantitative score that describes the degree of similarity between them. In this work, the ground-truth was created by averaging 10 noisy images acquired with normal radiation dose, as explained before.

One of the biggest problems related to denoising algorithms is the fact that normally they blur the image during the process of removing noise. Blurring is a big concern when working with medical images because it can impair de detection of subtle lesions, as microcalcifications, by radiologists. Thus, for image quality assessment we also consider the measurement of image sharpness. Sharpness is a non-reference image quality measurement and provides a measure related to the clarity of detail and edge definition of an image. We measured the sharpness of DBT images considering an extended gradient-based Tenengrad method proposed by He and Greenshields.[15]

2.5 Workflow of this study

This study was conducted based on the following procedures:

1. We calculated image quality assessment metrics for regions of interest (ROIs) of size 512 × 512 pixels, that includes one microcalcification cluster, extracted from all DBT projections acquired with the physical phantom at all radiation dose levels (100%, 85%, 70% and 50% dose image group). We measured the parameters for all 5 images (noise realizations) of each projection and averaged the results.
2. NLM and BM3D denoising algorithm was applied to all the projection images acquired in reduced radiation doses (i.e. 85%, 70% and 50%). Filtering parameters of both algorithms were adjusted to produce denoised images with the same quality (in terms of the objective metrics) of those acquired with the standard radiation dose (100% dose image group).
3. Image quality assessment metrics were calculated again for the ROI's extracted from the denoised projections, in order to evaluate the similarity between the images from different radiation dose after applying denoising.
4. Using the reconstruction software we obtained tomosynthesis slices of all radiation dose image groups.
5. Objective image quality assessment metrics were then calculated from the reconstructed slices, using ROIs of size 512 × 512 pixels extracted from 15 slices of each one of the image groups, including those generated after denoising.

3. RESULTS AND DISCUSSION

3.1 Analysis of tomosynthesis projections

Figure 1 shows the results of PNSR and MSSIM measurements for the DBT projections of each radiation dose sub-set, prior to the filtering process. Each value was calculated by averaging the results of five samples of each projection image. We can see in Figure 1 that the reduction in the radiation dose degrades the quality of DBT projections.

Table 1 shows the mean and standard deviation of PSNR and MSSIM measurements for all projections in its respective dose prior to denoising. The goal of our study is to filter the projections acquired with lower radiation doses (85% 70% and 50%) to achieve similar quality than the projections acquired with the standard dose (100%). Thus, we filtered all the projection images acquired with 85% 70% and 50% of the standard dose using both NLM and BM3D algorithms. The filter parameters for both algorithms, presented at last two columns of Table 1, were optimized in order to have a good noise removal with minimal blurring and also to approximate the values of PSNR and MSSIM to the values previously calculated for the images obtained with 100% of the dose.

(a) (b)

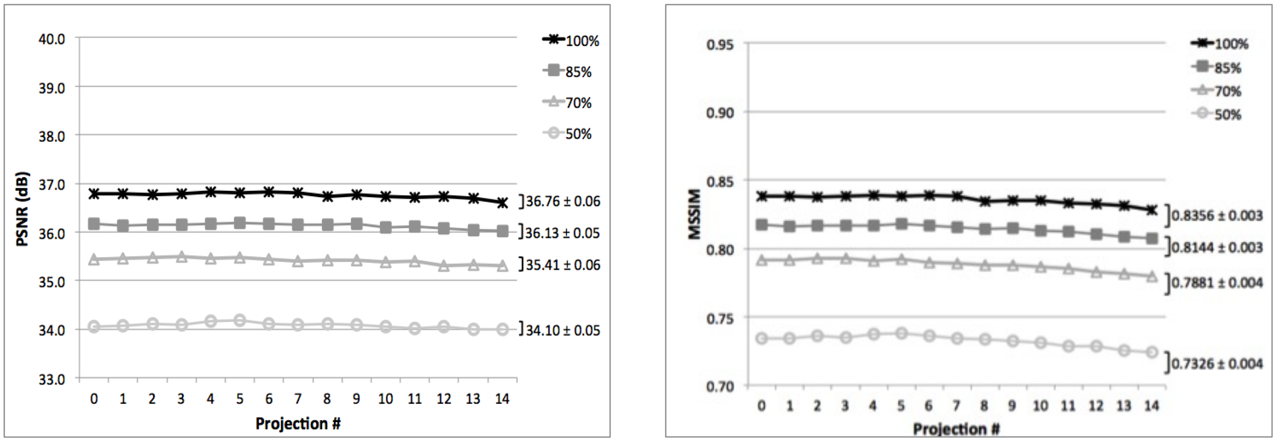

Figure 1 – (a) PSNR and (b) MSSIM average measurements calculated for projections images acquired at 100%, 85%, 70% and 50% of the standard radiation dose. Values in squared brackets are the mean and standard deviation calculated for all 15 projections in each dose. These values were used to adjust denoising parameters.

Table 1: PSNR and MSSIM mean and standard deviation values for all projections in each radiation dose prior to denoising. The last two columns show the parameters used for NLM and BM3D respectively to generate filtered projections with similar quality to the images acquired with 100% dose.

Radiation Dose	PSNR (dB)	MSSIM	$h_{(NLM)}$	$\sigma_{(BM3D)}$
100%	36.76 ± 0.06	0.830 ± 0.003	-	-
85%	36.13 ± 0.05	0.810 ± 0.003	0.0036	1.19
70%	35.41 ± 0.06	0.790 ± 0.004	0.0038	1.77
50%	34.07 ± 0.05	0.730 ± 0.004	0.0050	2.54

After denoising using both algorithms, all projections were evaluated again in terms of PSNR and MSSIM to confirm how close those images became of the normal dose. These results are presented at Figure 2 for the NLM and Figure 3 for the BM3D algorithms, respectively.

(a) (b)

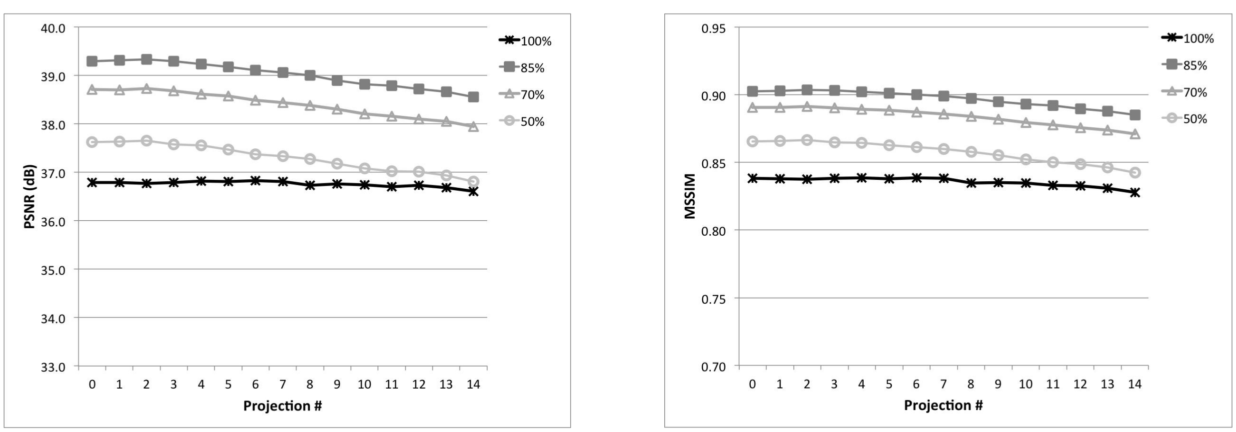

Figure 2 – Image quality assessment of the DBT projections in terms of (a) PSNR and (b) MSSIM after denoising by the NLM algorithm. We measured these parameters for all 5 images of each projection and averaged the results.

(a)

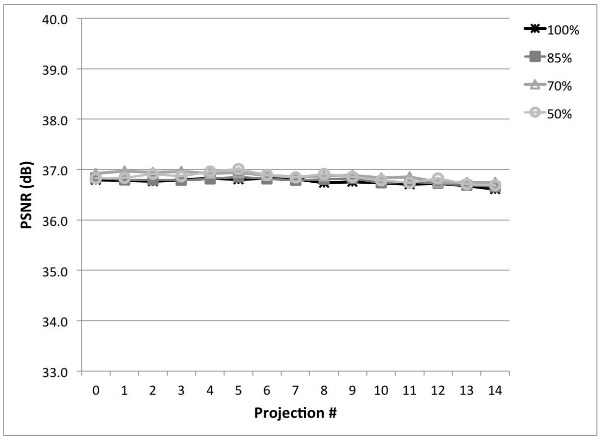

(b)

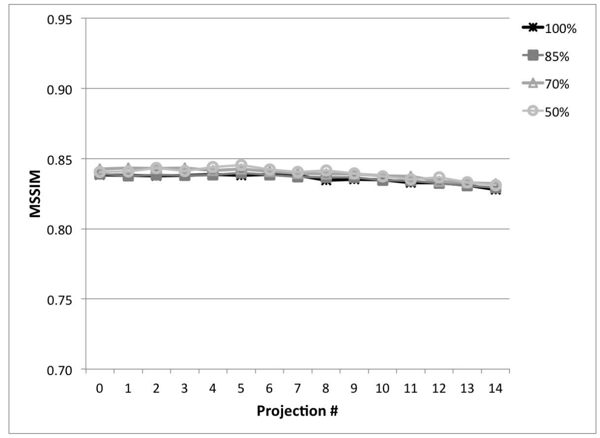

Figure 3 – Image quality assessment of the DBT projections in terms of (a) PSNR and (b) MSSIM after denoising by the BM3D algorithm. We measured these parameters for all 5 images of each projection and averaged the results.

As can be seen at Figures 2 and 3, the BM3D algorithm performed better noise adjustment than the NLM for the projections acquired with lower radiation doses. The mean difference in terms of PSNR measurements between projections acquired with full radiation dose and half dose, for example, was 2.68 dB (Figure 1). After denoising, the mean difference between PSNR measurements were reduced to 0.54 dB for the NLM and 0.09 dB for the BM3D algorithms. Thus, BM3D denoising was capable to remove noise from the low-dose projections to generate filtered images very similar to those acquired with the standard radiation dose. Regarding the NLM algorithm, it removed more noise than necessary to adjust the quantum noise level of the low-dose images.

Figure 4 shows one example of the results obtained with both denoising algorithms. The image on the left (a) shows a ROI (with a cluster of microcalcifications - size ranged from 850μm to 2000μm) extracted from the central projection acquired at 100% of the standard radiation dose. Image (b) shows the same ROI extracted from a projection acquired with 50% of the standard dose. Images (c) and (d) show the resulting image after denoising using NLM and BM3D algorithm, respectively. Images presented in Figure 4 show that the image acquired with 50% of dose reduction has more noise than the image acquired with the standard radiation dose, as expected. After applying the filtering procedure proposed in this work, this image become more similar to the 100% dose image and the microcalcifications were preserved.

(a) (b) (c) (d)

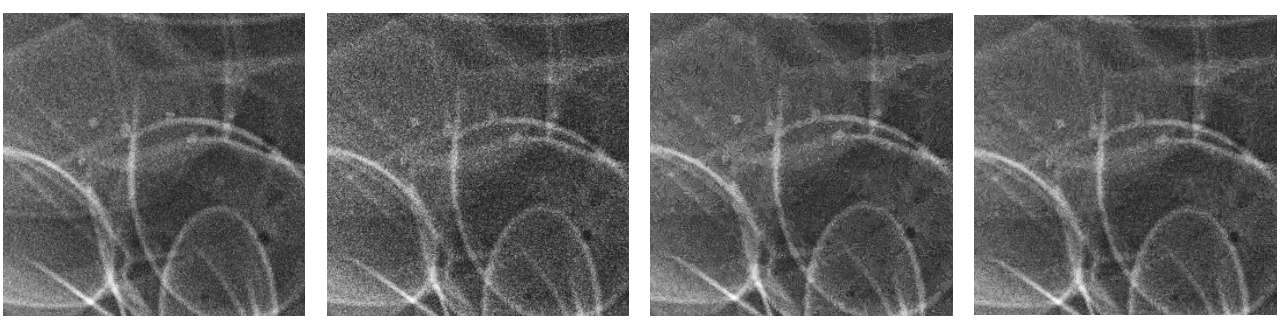

Figure 4 – ROIs showing a cluster of microcalcifications extracted from the central projection of the anthropomorphic breast phantom acquired at (a) standard radiation dose and (b) 50% of the standard dose. Images (c) and (d) show the same ROIs extracted from the image acquired with 50% of the standard dose after being filtered by the NLM and BM3D algorithms, respectively.

In addition to PSNR and MSSIM, we also measured the sharpness of all ROIs extracted from the projections images after denoising and compared to the sharpness of the full-dose image set, in order to evaluate how blurred become the filtered images, after denoising, compared to the images acquired with the standard radiation dose. Figure 5 shows the values of sharpness calculated for all projections acquired with lower radiation dose after being filtered by NLM and BM3D, compared to the ones acquired with full dose.

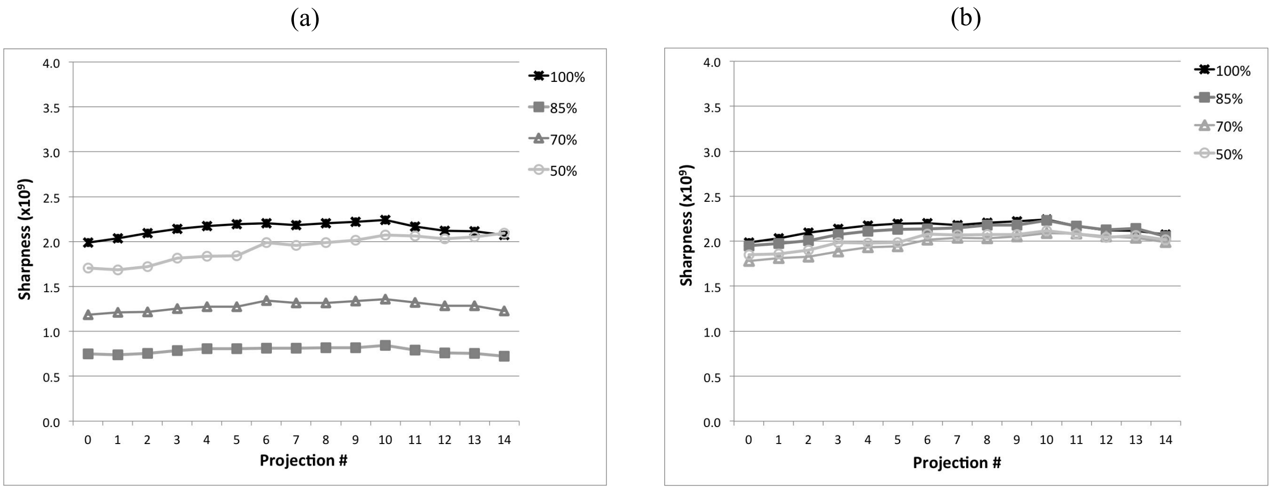

Figure 5 – Image quality assessment of the DBT projections in terms of sharpness after denoising by the (a) NLM and (b) BM3D algorithm. We measured these parameters for all 5 images of each projection and averaged the results.

Analyzing the results presented in Figure 5 we can observe that the BM3D removes noise with less blurring than the NLM algorithm. Considering a radiation dose reduction of 50%, for example, the mean difference in terms of sharpness after denoising, compared to the 100% dose image, was approximately 10.4% for the NLM and 6.1% for the BM3D algorithm.

3.2 Analysis of reconstructed tomosynthesis images

We used the reconstruction software, described previously, to generate tomographic slices of each image set. Then, following the same procedure we use to assess the projections before the reconstruction step, we also calculated the image quality assessment metrics for ROI's of size 512 × 512 pixels extracted from 15 DBT slices (slices #35-50) selected of all image sets, before and after denoising. Slices were selected to include the center slice where the microcalcification cluster was on focus with seven slices below and seven slices above the center slice, with a step of 1.0 mm. We measured the parameters for all 5 images (noise realizations) of each slice and averaged the results.

Thus, we could evaluate the influence of a reduction in the radiation dose, and also of the proposed denoising methodology, in the quality of the reconstructed DBT images. Figure 6 shows the results of PNSR and MSSIM measurements for the DBT slices of each radiation dose group, prior to the filtering process. Each value was calculated by averaging the results of five samples of each reconstructed tomographic slice.

Analyzing the graphs in Figure 6 we can notice that the reconstruction algorithm improved the quality of the DBT slices in comparison to the projections images (see Figure 1). Moreover, the slices reconstructed from lower dose projections are of less quality then the slices generated from projections acquired at standard radiation dose.

(a) (b)

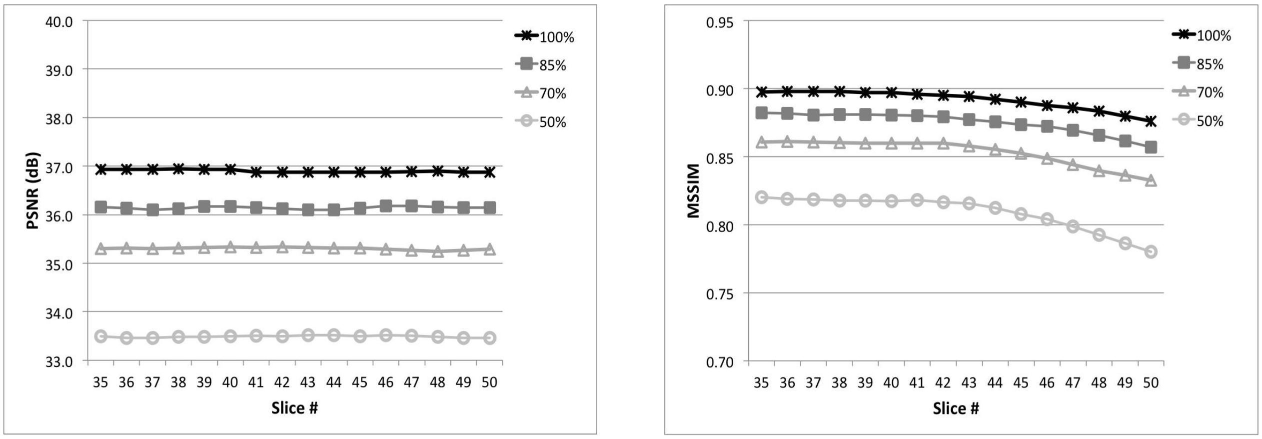

Figure 6 – PSNR and MSSIM calculated for ROIs extracted from 15 tomographic slices reconstructed from the projections acquired at 100%, 85%, 70% and 50% of the standard radiation dose (before denoising). We measured these parameters for all 5 images of each slice and averaged the results.

We reconstructed DBT slices using denoised projections and recalculated the image quality assessment for such reconstructed slices. Figure 7 and 8 show the results of PSNR and MSSIM measurements for the slices reconstructed from the projections denoised by NLM and BM3D algorithms, respectively. Each value was calculated by averaging the results of five samples of each one of 15 selected tomographic slices, as explained previously.

(a) (b)

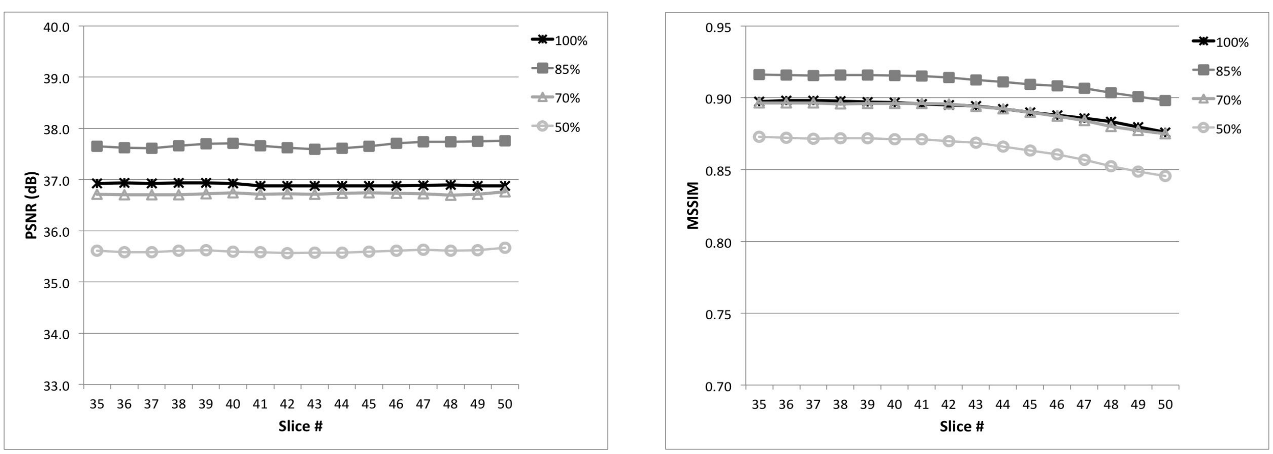

Figure 7 – PSNR and MSSIM measurements calculated for 15 ROIs extracted from tomographic slices reconstructed with low-dose projections acquired at 85%, 70% and 50% of the standard radiation dose, after being filtered by NLM algorithm. We measured these parameters for all 5 images of each slice and averaged the results.

(a) (b)

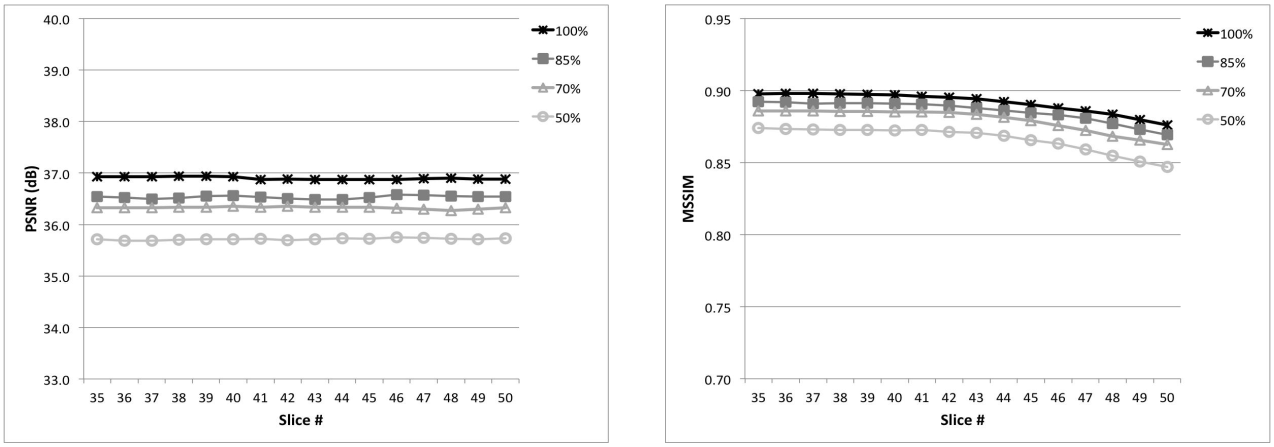

Figure 8 – PSNR and MSSIM measurements calculated for 15 ROIs extracted from tomographic slices reconstructed with low-dose projections acquired at 85%, 70% and 50% of the standard radiation dose, after being filtered by BM3D algorithm. We measured these parameters for all 5 images of each slice and averaged the results.

Results presented in Figures 7 and 8 show that BM3D algorithm, again, achieved better noise adjustment than the NLM for the slices reconstructed from projections acquired with lower radiation doses. However, although the image quality between projections had been very similar after BM3D filtering, as seen in Figure 3, after the reconstruction the similarity was not so high. Before denoising, the mean difference in terms of PSNR measurements between projections acquired with full radiation dose and half dose, for example, was 3.41 dB (Figure 6). After denoising, the mean difference between PSNR measurements was reduced to 1.30 dB for the NLM and 1.18 dB for the BM3D algorithm. We believe that optimizing the combination of the reconstruction and denoising methods may achieve a further improvement in image quality. Such an optimization is objective of our future work.

Figure 9 shows one example of the results of reconstructed slices obtained with both denoising algorithms. The image on the left (a) shows a ROI (with a cluster of microcalcifications ranging from 850μm to 2000μm) extracted from a slice reconstructed from projections acquired at 100% of the standard radiation dose. Image (b) shows the same ROI extracted from a slice generated from projections acquired with 50% of the standard dose. Images (c) and (d) show slices from projections acquired with 50% dose after being filtered by NLM and BM3D algorithm, respectively. Images presented in Figure 9 show that the slices from projections acquired with 50% of dose have more noise than the slices from standard radiation dose, as expected. After applying denoising, slices from filtered projections become more similar to the 100% dose image and the microcalcifications were preserved.

(a) (b) (c) (d)

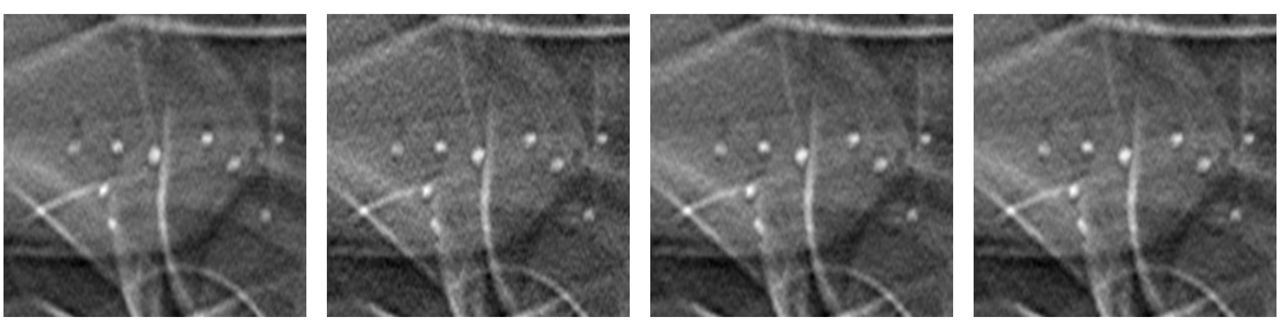

Figure 9 – ROIs showing cluster of microcalcifications extracted from DBT slices of the anthropomorphic breast phantom reconstructed from projections acquired at (a) standard radiation dose and (b) 50% of the standard dose. Images (c) and (d) show the same ROIs extracted from slices reconstructed using projections acquired with 50% of the standard dose after being filtered by the NLM and BM3D algorithms, respectively.

Finally, we measured the sharpness of all ROIs extracted from the selected slices after denoising and compared to the sharpness calculated for the slices of the full-dose image set, in order to evaluate how blurred become the slices which were reconstructed from denoised projections, compared to the images acquired with the standard radiation dose. Figure 10 shows the values of sharpness calculated for all slices from projections acquired with lower radiation dose after being filtered by NLM and BM3D, compared to the ones acquired with full dose.

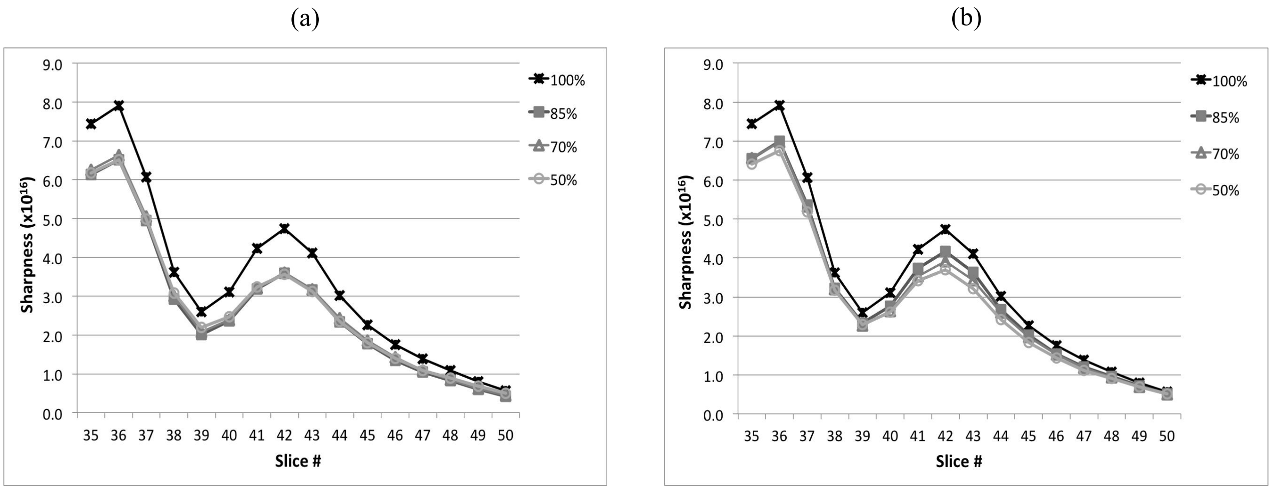

Figure 10 – Image quality assessment of the reconstructed slices in terms of sharpness after the projections being denoised by the (a) NLM and (b) BM3D algorithm. We measured these parameters for all 5 images of each slice and averaged the results.

Slices reconstructed from projections acquired with lower radiation dose, after being filtered by the BM3D algorithm, were slightly less blurred (in terms of the calculated sharpness measure) than those filtered by the NLM algorithm. However, the mean difference in terms of sharpness, after denoising, between the low-dose and the 100% dose images increased after reconstruction. Considering a radiation dose reduction of 50%, for example, the mean sharpness differences have increased to approximately 18.9% for the NLM and 16.2% for the BM3D algorithms.

4. CONCLUSIONS

In this work we investigated the use of "state of the art" denoising algorithms to allow dose reduction in DBT. Projections images were acquired on a clinical DBT machine at different dose levels, using an anthropomorphic breast phantom with inserted simulated microcalcifications. We processed all projections acquired with reduced dose using both NLM and BM3D algorithms aimed at reaching the same image quality as standard-dose images. This way, reduced doses improve patient safety while denoising help maintain high image quality.

Assessment using image quality metrics such as PSNR and MSSIM showed that both denoising algorithms could filter projections acquired at the reduced radiation dose. However, BM3D algorithm achieved better noise adjustment (mean difference in peak signal to noise ratio < 0.1 dB) than the NLM for the projections acquired with lower radiation doses. Moreover, BM3D removed the noise with less blurring, measured in terms of sharpness, than the NLM algorithm (mean difference in image sharpness ~ 6%). NLM removed more noise than necessary to adjust the quantum noise level of the low-dose images because the algorithm does not work properly if you use very small values of *h*. In this case, the adjustment was not so perfect and the filter over denoised the projections.

After reconstruction, similar results were achieved. Reconstructed slices from denoised projections were very similar to slices reconstructed from the projections acquired with standard radiation dose. However, the similarity was not so high than achieved for the projections (mean difference in peak signal to noise ratio ~ 1.2 dB), because the reconstructing algorithm modified the noise characteristics of the images. In the case of reconstructed slices, again, BM3D filter performed better noise adjustment than NLM algorithm.

Some of the limitations of this paper and future directions are now addressed. One limitation is that all DBT images used in this study were acquired using a physical breast phantom. We chose to use phantom images because this allows us to acquire several DBT images with different radiation doses without concern about patient's absorbed radiation exposures and without inserting movement artifacts in our images. However, a further study using clinical data must be conducted to properly evaluate the possibility of using denoising techniques to reduce dose in DBT imaging.

ACKNOWLEDGMENTS

The authors would like to thank Ms. Susan Ng from Real-Time Tomography, LLC (Villanova, PA) for providing us the Briona™ 3D reconstruction software to generate all tomographic slices used in this study.

This work was supported by the São Paulo Research Foundation (FAPESP) grant #2013/18915-5, by the Brazilian Foundation for the Coordination of Improvement of Higher Education Personnel (CAPES) and by the US National Institutes of Health (NIH): R01 grant #CA154444. The content is solely the responsibility of the authors and does not necessarily represent the official views of the NIH, CAPES or FAPESP.

REFERENCES

[1] Sechopoulos, I., "A review of breast tomosynthesis. Part I. The image acquisition process.," Med. Phys. **40**(1), 014301 (2013).

[2] Baker, J. A., Lo, J. Y., "Breast tomosynthesis: state-of-the-art and review of the literature.," Acad. Radiol. **18**(10), 1298–1310 (2011).

[3] "FDA Device Approvals and Clearances. U.S. Food and Drugs Administration.", 2011, <http://www.fda.gov/MedicalDevices/ProductsandMedicalProcedures/DeviceApprovalsandClearances/default.htm > (15 January 2015).

[4] Hendrick, R. E., "Radiation doses and cancer risks from breast imaging studies.," Radiology **257**(1), 246–253 (2010).

[5] Yaffe, M. J., Mainprize, J. G., "Risk of radiation-induced breast cancer from mammographic screening.," Radiology **258**(1), 98–105 (2011).

[6] Ruschin, M., Timberg, P., Båth, M., Hemdal, B., Svahn, T., Saunders, R. S., Samei, E., Andersson, I., Mattsson, S., et al., "Dose dependence of mass and microcalcification detection in digital mammography: free response human observer studies.," Med. Phys. **34**(February), 400–407 (2007).

[7] Huda, W., Ogden, K. M., Scalzetti, E. M., Dance, D. R., Bertrand, E. A., "How Do Lesion Size and Random Noise Affect Detection Performance in Digital Mammography?," Acad. Radiol. **13**(5), 1355–1366 (2006).

[8] Buades, A., Coll, B., Morel, J. M., "A Review of Image Denoising Algorithms, with a New One," Multiscale Model. Simul. **4**(2), 490–530 (2005).

[9] Dabov, K., Foi, A., Katkovnik, V., Egiazarian, K., "Image Denoising by Sparse 3-D Transform-Domain Collaborative Filtering," IEEE Trans. Image Process. **16**(8), 2080–2095 (2007).

[10] Cockmartin, L., Bakic, P., Bosmans, H., Maidment, A. A., Gall, H., Zerhouni, M., Marshall, N., "Power Spectrum Analysis of an Anthropomorphic Breast Phantom Compared to Patient Data in 2D Digital Mammography and Breast Tomosynthesis," Lecture Notes in Computer Science Volume 8539 (Breast Imaging), H. Fujita, T. Hara, and C. Muramatsu, Eds., Springer International Publishing, 423–429 (2014).

[11] Pokrajac, D. D., Maidment, A. D. A., Bakic, P. R., "Optimized generation of high resolution breast anthropomorphic software phantoms.," Med. Phys. **39**(4), 2290–2302 (2012).

[12] Kuo, J., Ringer, P. A., Fallows, S. G., Bakic, P. R., Maidment, A. D. A., Ng, S., "Dynamic Reconstruction and Rendering of 3D Tomosynthesis Images," SPIE Med. Imaging **7961**, 796116–796116 – 11 (2011).

[13] Wang, Z., Bovik, A. C., "Mean squared error: Love it or leave it? A new look at signal fidelity measures," IEEE Signal Process. Mag. **26**(January), 98–117 (2009).

[14] Wang, Z., Bovik, A. C., Sheikh, H. R., Simoncelli, E. P., "Image quality assessment: From error visibility to structural similarity," IEEE Trans. Image Process. **13**(4), 600–612 (2004).

[15] He, L., Greenshields, I. R., "A nonlocal maximum likelihood estimation method for Rician noise reduction in MR images," IEEE Trans. Med. Imaging **28**(2), 165–172 (2009).